www.elsevier.nl/locate/elecom

Electrochemistry Communications 1 (1999) 453–458

electrochemistry communications

Determination of heterogeneous electron transfer rate constants at microfabricated iridium electrodes

Rosemary Feeney, Samuel P. Kounaves *

Tufts University, Department of Chemistry, Medford, MA 02155, USA

Received 26 July 1999; received in revised form 4 August 1999; accepted 5 August 1999

Abstract

There has been an increasing use of both solid metal and microfabricated iridium electrodes as substrates for various types of electroanalysis. However, investigations to determine heterogeneous electron transfer rate constants on iridium, especially at an electron beam evaporated or dc magnetron sputtered surface, have not previously been performed. This paper compares the results of these microfabricated surfaces using ultramicroelectrode arrays and steady-state currents. Even though the dc magnetron sputtered iridium surface demonstrated a slightly more reversible electrochemical behavior than the electron beam evaporated surface, overall the microfabricated microelectrodes and ring electrode indicated similar reversibility to the polished metallic iridium disk electrode.

Keywords: Iridium; Rate constant; Steady-state current; Ferricyanide; Microfabrication

1. Introduction

Macro- and microelectrodes of all shapes and sizes have been fabricated from a variety of materials, but most often from platinum and gold wires or glassy carbon rods and fibers. Recently, there has been increase in the use of both metallic and microfabricated iridium-based electrodes for a variety of electroanalytical techniques [1–12]. Before being used, solid metallic poly-crystalline electrodes are polished and treated chemically and/or electrochemically to improve their electroanalytical response. Microlithographically fabricated ultramicroelectrodes (UMEs) have become popular because they can provide micron-sized, highly accurate and reproducible surfaces, especially for arrays of ultramicroelectrodes (UMEAs). However, a perceived drawback to these types of electrodes has been the inability to polish or effectively regenerate the original surface. The most visible effect of the polishing procedure is on the electron transfer rate. A smooth polished surface is considered indispensable in providing fast and easy transfer of electrons between the electrode and the analyte redox species. The heterogeneous electron transfer rate constants are usually measured using voltammetric and impedance based methods with redox species such as ferricyanide and ferrocene, both of which undergo a standard one-electron transfer process and exhibit reversible behavior often highly dependent on the pretreatment of the electrode surface. For platinum and gold microelectrodes, where rates are usually two orders of magnitude faster, several groups have reported using fast-scan cyclic voltammetry to successfully make such measurements [13–18]. However, to date there have been no reported investigations of heterogeneous electron transfer rate constants for any type of iridium-based electrodes.

Rate constants at macroelectrodes are typically calculated using the well-known Nicholson method, which is based on the amount of peak separation between the forward and reverse scans in a cyclic voltammogram [19]. The methodology however is susceptible to errors resulting from ohmic polarization and charging currents, which can lead to overstated rate constants. Alternatively, steady-state voltammetry is a powerful method to study electrode processes, by being able to directly measure rapid heterogeneous rate constants [20–23]. By using ultramicroelectrodes, advantages such as steady-state currents, increased mass transport, and the ability to be used in highly resistive media, can be obtained. Moreover, there is minimal iR_u drop and low background currents associated with ultramicroelectrodes. The steady-state current is a result of the radial diffusion at the ultramicroelectrode. The resulting voltammogram is sigmoidally shaped and under reversible conditions the half-wave potential $E_{1/2}$ occurs at the reversible half-wave potential E_h:

* Corresponding author. Tel.: +1-617-627-3124; fax +1-617-627-3443;

1388-2481/99/$ - see front matter
PII S1388-2481(99)00091-0

$$E_h = E^\circ + \left(\frac{RT}{nF}\right)\ln\left(\frac{D_R}{D_O}\right)$$

and when the diffusion coefficients of the reduced and oxidized species (D_R and D_O, respectively) are equal, we have $E_h = E^\circ$. The equation that describes the reversible voltammogram is identical with a typical reversible polarographic wave when the diffusion coefficients are equal, and the plot of $\log[i/(i_d - i)]$ versus E can be used to evaluate the experimental data (where E is the electrode potential, i is the current, and i_d is the diffusion controlled limiting current) [13,23]. A slope of less than RT/nF is an indication that there is competition between kinetic and diffusion control and that it is a quasi-reversible system.

In the work reported here, rate constants for ferricyanide and ferrocene were calculated using cyclic voltammetry and the Nicholson method at a solid iridium disk electrode, as well as untreated iridium electrodes that were prepared using electron-beam evaporation and dc magnetron sputtering. Peak potential separations (ΔE_p) were measured at several microfabricated electrodes over several days. In addition, steady-state currents were used to calculate rate constants at ultramicroelectrode arrays prepared by electron beam evaporation or dc magnetron sputtering.

2. Experimental

2.1. Apparatus

A model 263 potentiostat/galvanostat (EG&G PAR, Princeton, NJ) interfaced to a DEC p420-SX microcomputer using model 270 software (EG&G) was used to apply techniques and collect the data. All voltammetric experiments were carried out in a Faraday cage using a three-electrode cell comprising the working electrode and either a Ag|AgCl (3 M NaCl) reference electrode and Pt wire counter electrode for the aqueous media experiments, or a large Ag wire (99.99%) pseudo-reference and Pt wire for the non-aqueous experiments. All experiments were carried out at 298 K. Nitrogen gas was used to deoxygenate the DMSO. All potentials are reported versus the Ag|AgCl (3 M NaCl) reference electrode.

2.2. Working electrodes

Five different types of working electrodes were used. A solid iridium inlaid disk microelectrode (MICRO#1) was fabricated using a 127 μm diameter iridium wire heat-sealed in a glass sheath with a copper wire soldered to the iridium to make the electrical connection [11]. A microfabricated ring electrode (RING#1) and three ultramicroelectrode arrays (UMEA#1–#3) were made using standard microlithographic techniques by electron-beam evaporation (e-beam E) or dc magnetron sputtering (dcMS) to deposit approximately 2000–3000 Å of iridium onto an oxidized silicon wafer. The fabrication processes have been previously described in detail [1,4–6,10].

The ring electrode (RING#1), shown in Fig. 1, consisted of a 140 μm wide ring with an outer diameter of approximately 2.5 mm. The area, determined chronoamperometrically using ferricyanide, was found to be 5.1×10^{-3} cm^2. The

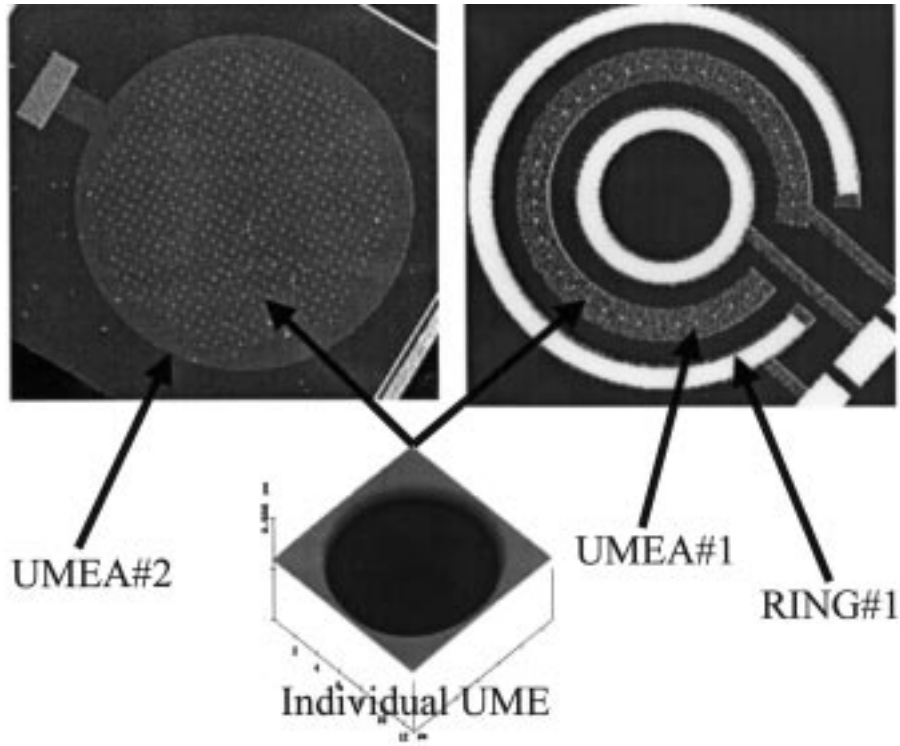

Fig. 1. SEM images of the microfabricated UME arrays (UMEA#1, UMEA#2, RING#1) and an AFM image of an individual UME.

Table 1
Dimensions of electrodes determined electrochemically using potassium ferricyanide in KNO_3 and a potential step experiment

	Area/10^3 cm^2	Diameter/μm
MICRO#1 Ir-disk	0.126	127
RING#1 e-beam evap.	5.11	
UMEA#1 e-beam evap.	0.0249	8.9
UMEA#2 e-beam evap.	0.110	8.9
UMEA#3 dcM sputtered	0.015	10

UME arrays consisted of 177 (UMEA#2, e-beam E) elements arranged in a honeycomb pattern (Fig. 1), 40 (UMEA#1, e-beam E) elements arranged on the same chip as the ring electrode arranged in a ring pattern (Fig. 1), or 20 (UMEA#3, dcMS) elements arranged in a 5×4 array. In all cases the individual ultramicroelectrodes were 10 μm in diameter. Dimensions for the UMEs were also verified with an atomic force microscope (Nanoscope-E, Digital Instruments). Their dimensions and areas are summarized in Table 1.

The microelectrode (MICRO#1) was polished with 400 grit, then 30, 6, 1, and 0.25 μm diamond paste (Buehler, Lake Bluff, IL) on a carbimet-polishing pad. It was sonicated in deionized water containing 5 ml Micro® cleaning solution (International Products, Burington, NJ) and then in pure deionized water for an additional 2 min. All the microfabricated electrodes UMEA#1–UMEA#3 and RING#1 were used as received (Fig. 2).

2.3. Measurements

For the MICRO#1 and RING#1 electrode, cyclic voltammetry was used with a scan rate of 3.5 V s^{-1}, a 6 mV scan increment, and a step time of 0.0017 s. Data were collected using the UMEAs at a scan rate of 0.1 V s^{-1}, 2 mV scan increment, and a step time of 0.2 s. The potential window was 0.5 to -0.3 V in KNO_3 and 0.15 to 0.89 V for DMSO. The switching potential was kept constant throughout the experiments. Background currents and iR_u drop, which tend to distort voltammograms as a result of charging currents and double-layer capacitance, are usually minimized by the use of ultramicroelectrodes. However, to insure a more accurate measure of faradaic current, supporting electrolyte concentrations were kept at 1 M, a three-electrode electrochemical cell was used, and background subtractions were made using data from a cell containing only supporting electrolyte. An *IR* compensation of 50 Ω was used with the RING#1 electrode during the non-aqueous experiments.

Diffusion coefficients for the ferricyanide and ferrocene redox couples, determined by chronoamperometry at a Au disk macroelectrode of 3 mm diameter using a 10 s time scale, were calculated to be 7.71×10^{-6} and 1.88×10^{-5} cm^2 s^{-1} respectively.

2.4. Solutions

The aqueous electrolytes consisted of 6.0, 1.0, and 0.6 mM concentrations of potassium ferricyanide (Sigma) in 1.0 M potassium nitrate (EM Science). The non-aqueous electrolyte consisted of 1 mM ferrocene solution (Aldrich) and 0.5 M tetrabutylammonium hexafluorophoshate (Aldrich) in dimethyl sulfoxide (DMSO, Aldrich). All chemicals were reagent grade and solutions were prepared using 18 MΩ cm deionized water from a Barnstead Nanopure system (Barnstead Co., Dubuque, IA).

3. Results and discussion

3.1. Microfabricated ring electrode (RING#1)

The Nicholson method [19] was used to evaluate the rate constant (k) at both MICRO#1 and RING#1 electrodes.

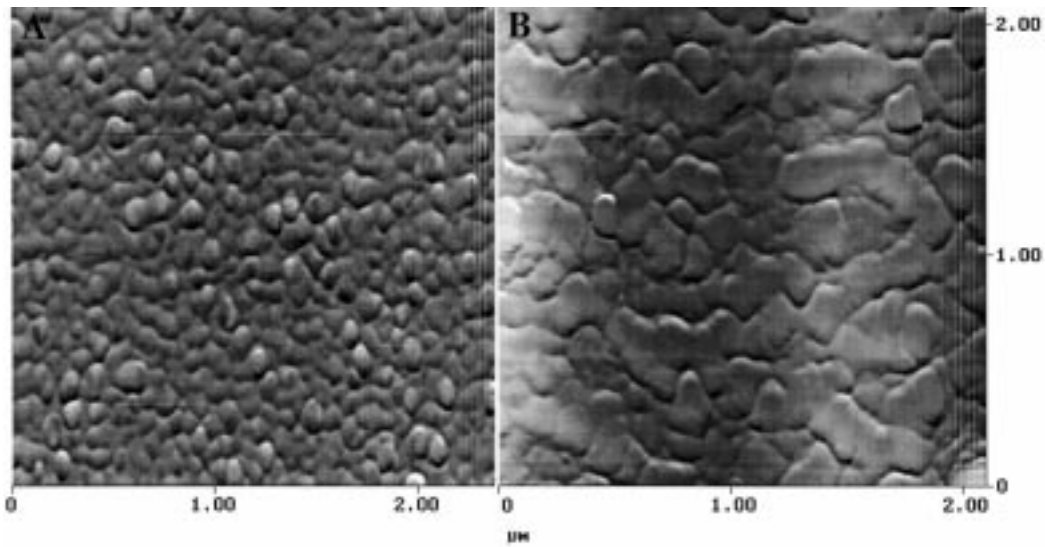

Fig. 2. AFM images of the iridium (A) e-beam evaporated (UMEA#1) and (B) dc magnetron sputtered (UMEA#3) surfaces.

Anodic and cathodic peak separations from a background-subtracted voltammogram were used to evaluate ψ from which k was obtained using the expression:

$$\psi = \frac{k}{(aD_O)^{1/2}}$$

where D_O is the diffusion coefficient and $a = nF\nu/RT$ (ν being the scan rate). For this experiment $\nu = 3.5$ V s^{-1} and thus linear diffusion should dominate. Table 2 shows the results for k for MICRO#1 and RING#1. The e-beam evaporated surface of RING#1 yielded a rate constant the same as that for the polished surface of MICRO#1 for ferricyanide, even though the surface of RING#1 was not pretreated in any way. Multiple runs resulted in minimal deviation (standard deviations for an individual electrode were small). These data suggest that both types of surfaces are apparently equivalent in terms of nature and morphology.

However, for ferrocene, the RING#1 electrode yielded a lower rate constant in DMSO. Even though the supporting electrolyte concentration used was 500 times greater than that of ferrocene, some uncompensated resistance may still remain in the cell. This resistance would shift the cathodic and anodic peak potentials so that larger peak separations (ΔE_p) would result with an increase in scan rate. Additional *IR* compensation was attempted, but ΔE_p never attained a value of below 96 mV. Since we do not know of any reports in the literature investigating the utility of microfabricated electrodes in non-aqueous environments, a more thorough investigation may be warranted.

To demonstrate that the peak potential response at the iridium surface is stable, ΔE_p was measured using RING#1 in 6 mM ferricyanide and 1 M KNO_3 over several days. Table 3 shows the average values obtained over the course of the study. The data show a consistent and uniform response for all the UMEAs. The ΔE_p value is very similar to that of the solid iridium electrode MICRO#1 which had been carefully treated and polished using diamond paste prior to use.

To test the effects of a pretreatment on ΔE_p, RING#1 was subjected to both an electrochemical (cyclic voltammetry in a 0.1 M perchloric acid solution) and chemical (concentrated and 3 M sulfuric and nitric acids) pretreatment. No significant qualitative change was observed and an average $\Delta E_p = 80.9$ mV was measured with the smallest separation attained being $\Delta E_p = 74.4$ mV. It should be noted that after a week of constant use, ΔE_p did increase, in some cases up to 125 mV. Degradation of the thin iridium surface is a possible cause. However upon applying a drop of concentrated nitric acid for 30 s, ΔE_p was reduced to below 90 mV. In this way, partial restoration of the response could be achieved.

3.2. Ultramicroelectrode arrays (UMEA#1–#3)

For the evaluation of k on the ultramicroelectrode arrays, the method used by Oldham et al. [22] was applied with k given by the expression:

Table 2
Rate constants for the Ir-disk and microfabricated electrodes

	k for ferricyanide/ cm s^{-1}	k for ferrocene/ cm s^{-1}
MICRO#1 Ir-disk	0.0717 ± 0.0214	0.197 ± 0.044
RING#1 e-beam evap.	0.0739 ± 0.0131	0.0606 ± 0.0147

Table 3
Peak potential separations for evaporated Ir UMEA#2. Averages were 84.7 ± 7.0, 82.9 ± 7.1, and 84.7 ± 5.6, respectively. Data obtained using RING#1 with 6 mM ferricyanide in KNO_3 ($n = 11$)

Day	UMEA#1/ mV	UMEA#2/ mV	UMEA#3/ mV	MICRO#1/ mV
1	84.0 ± 2.0	79.9 ± 1.4	82.1 ± 2.5	82.7 ± 2.0
2	82.1 ± 1.1	82.6 ± 4.5	83.0 ± 2.6	
3	89.0 ± 4.6	80.0 ± 4.5	87.1 ± 4.1	
4	87.3 ± 4.9	89.1 ± 3.2	86.7 ± 1.2	

$$1 - \exp\left[\frac{nF(E_{1/2} - E_h)}{RT}\right] = \frac{2D_O}{ka}$$

where $E_{1/2}$ is the experimental half-wave potential and E_h is the reversible half-wave potential. The value of k for the UMEAs was calculated using $E_h = 0.117$ V and $T = 298$ K. Current–potential curves were generated by plotting $\log[i/(i_d - i)]$ versus E (Fig. 3). Theoretically, the data for a reversible system should yield a straight line for which the inverse slope equals 59.2 mV. A linear relationship was found for all UMEAs tested as shown in Table 4. Fig. 4 shows typical steady-state cyclic voltammograms (CVs) obtained for the three electrode types. The CVs were recorded using 6 mM ferricyanide in 1 M KNO_3 with a scan rate of 0.1 V s^{-1} for electrodes UMEA#1 (· · ·), UMEA#2 (———) and UMEA#3 (- - -). Currents for UMEA#1 and #3 were multiplied by a factor of 5 and 8, respectively, for comparison to UMEA#2. The forward slopes for all three are basically the

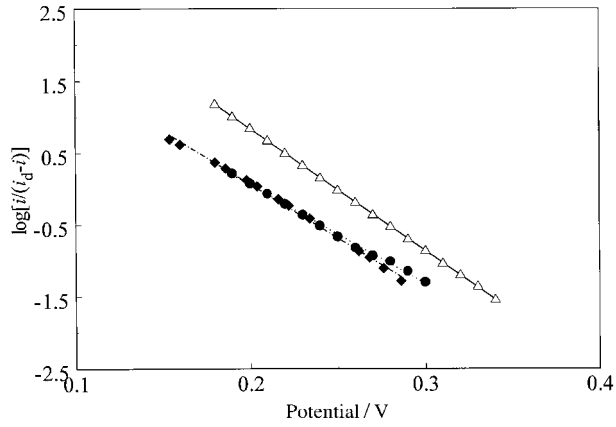

Fig. 3. Conventional log plots using 6 mM ferricyanide in 1 M KNO_3 with a scan rate of 0.1 V s^{-1} using the e-beam evaporated UMEA#1 (♦), e-beam evaporated UMEA#2 (●), and dc magnetron sputtered UMEA#3 (△) electrodes.

Table 4
Linear regression results for Ir UMEAs

	Regression coefficient (R^2)	Average slope/mV	Average intercept
UMEA#1 e-beam evap.	0.998	73 ± 2	3.05
UMEA#2 e-beam evap.	0.995	73 ± 2	2.66
UMEA#3 dcM sputtered	0.999	59 ± 2	4.27

same. Some hysteresis is evident in the voltammogram resulting from the possible presence of a stray capacitive current.

In order to insure that the UME arrays exhibited minimal overlap of the diffusion layer, the dominant mode of diffusion at a microdisk electrode was evaluated using the dimensionless parameter, p, which is related to the radius of the electrode, r, the scan rate, ν, and the diffusion coefficient of the electroactive species, D, as follows:

$$p = \left[\frac{nFr^2\nu}{RTD}\right]^{1/2}$$

At values of $p < 0.6$ radial diffusion dominates while at values of $p > 17$ linear diffusion dominates [24]. For microdisk arrays, assuming the UMEs are spaced far enough apart, the steady-state limiting current I_d is given by $I_d = 4mnFDCr$, where r is the radius of the microdisk, and m is the number of microelectrodes [25,26]. This expression holds true when $Dt/r^2 > 100$ and the separation between microelectrodes is greater than 10 times the diameter. The smallest separation for the arrays used in this study is 10 times the diameter. Since the radius of one UME is equal to 5×10^{-4} cm then p would be 0.35, which is consistent with radial diffusion. If however, there was diffusional overlap, the combined radius would be equal to 0.0787 cm (UMEA#1) yielding a p of 8.8 (the average of 17 and 0.6), which suggests a deviation from both types of diffusion. To examine whether a total steady-state current was obtained, a CV was obtained in a stirred solution using the UMEA#2. The separation between forward and

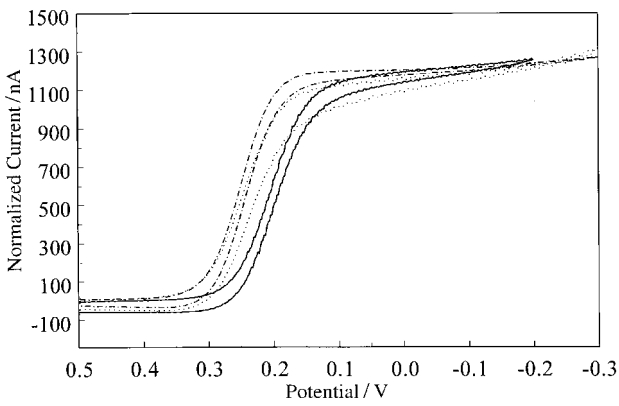

Fig. 4. CVs of 6 mM ferricyanide in 1 M KNO_3 with a scan rate of 0.1 V s^{-1} using UMEA#1 (· · ·), UMEA#2 (———), and UMEA#3 (- - -). Currents for UMEA#1 and #3 were multiplied by a factor of 5 and 8, respectively, for comparison with UMEA#2.

Table 5
Average rate constants using Ir UMEAs ($n = 10$)

	k for ferricyanide/ cm s^{-1}	k for ferrocene/ cm s^{-1}
UMEA#1 e-beam evap.	0.0423 ± 0.00076	0.0868 ± 0.00025
UMEA#2 e-beam evap.	0.0434 ± 0.0042	na
UMEA#3 dcM sputtered	0.0345 ± 0.0013	$0.0769 + 0.0002$

reverse scans decreased slightly and the limiting current increased slightly (7.5%) upon stirring. This suggested that a total steady-state current was not completely achieved. In this case, only a fraction of the diffusion current can be attributed to a linear component. However, only the forward scan is used in the data analysis.

3.3. Comparison

Using the results in Table 5, all arrays yield very similar rate constants, as the UME radii are nearly identical. The sputtered Ir array UMEA#3 had a reciprocal slope of 60.7 mV suggesting a reversible behavior. The deviation from the theoretical value is 1.5 mV. The cathodic transfer coefficient, α, was calculated to be 0.58 for the UMEAs, which is very similar to the theoretical cathodic transfer coefficient of 0.5 or literature value of 0.58 for a reversible $[Fe(CN)_6]^{3-} \leftrightarrow [Fe(CN)_6]^{4-}$ system at a platinum microelectrode [14]. This suggests a nearly reversible system. However in contrast, the reciprocal slopes for the evaporated Ir arrays show larger deviations from the theoretical value of 59.2 mV, suggesting a quasi-reversible behavior.

Rate constants in Table 5 are consistent with the values obtained at platinum microelectrodes using ferricyanide (0.07 cm s^{-1} [14] and 0.066 cm s^{-1}) [27]. In general, the rate constants for ferrocene were greater than those for ferricyanide and were also consistent with the literature value of 0.11 cm s^{-1} [13,18]. Reciprocal slopes of the conventional log plot analysis showed a deviation of only 5 mV from the theoretical value. Thus, ferrocene shows reasonably good reversibility at the microfabricated iridium electrodes used in this study.

4. Conclusions

Heterogeneous electron transfer rate constants for ferricyanide and ferrocene were calculated using the Nicholson method at a solid iridium substrate as well as at a surface prepared using electron beam evaporation. Peak potential separations at the electron beam evaporated iridium surface demonstrated reproducibility and uniformity among several different microfabricated electrodes over a four-day period. Also, rate constants were calculated for ultramicroelectrode arrays using steady-state currents. The dc magnetron sputtered surface behaved more reversibly and could be correlated

to theoretical values better than the e-beam evaporated surface. Thus, it appears that microfabrication techniques allow for metal surfaces to be prepared that are nearly identical in terms of electron transfer kinetics to a solid polycrystalline metallic surface that has been carefully polished and treated. The rate constants determined for ferricyanide and ferrocene at the iridium microelectrode (MICRO#1) were comparable to literature values for a platinum microelectrode.

Acknowledgements

This work was supported in part by grants from the US Environmental Protection Agency through the Northeast Hazardous Substance Research Center at NJIT and the National Science Foundation (CHE-9256871). The authors would like to thank Anthony Flannery at Stanford University's Center for Integrated Systems and Jim Doyle at the IBM Watson Research Center for fabricating the iridium arrays used for this work.

References

[1] M.A. Nolan, S.P. Kounaves, Anal. Chem. 77 (1999) 3567.
[2] P.R. Silva, M.A. El Khakani, M. Chaker, G.Y. Champagne, J. Chevalet, L. Gastonguay, R. Lacasse, M. Ladouceur, Anal. Chim. Acta 385 (1999) 249.
[3] C. Agra-Gutierrez, M.F. Suarez, R.G. Compton, Electroanalysis 11 (1999) 16.
[4] R. Feeney, J. Herdan, M.A. Nolan, S.H. Tan, V.V. Tarasov, S.P. Kounaves, Electroanalysis 10 (1998) 89.
[5] S.H. Tan, S.P. Kounaves, Electroanalysis 10 (1998) 364.
[6] J. Herdan, R. Feeney, S.P. Kounaves, A.F. Flannery, C.W. Storment, G.T.A. Kovacs, R.B. Darling, Environ. Sci. Technol. 32 (1998) 131.
[7] C. Belmont, M. Tercier, J. Buffle, G. Fiaccabrino, M. Koudelka-Hep, Anal. Chem. 70 (1998) 2949.
[8] A. Uhlig, U. Schnakenberg, R. Hintsche, Electroanalysis 9 (1997) 125.
[9] J. Wang, B. Tian, M. Jiang, Anal. Chem. 69 (1997) 1657.
[10] S.P. Kounaves, W. Deng, P.R. Hallock, G.T.A. Kovacs, C.W. Storment, Anal. Chem. 66 (1994) 418.
[11] S.P. Kounaves, W. Deng, Anal. Chem. 65 (1993) 375.
[12] S. Kounaves, W. Deng, J. Electroanal. Chem. 301 (1991) 77.
[13] A. Bond, T. Henderson, D. Mann, T. Mann, W. Thormann, C. Zoski, Anal. Chem. 60 (1988) 1878.
[14] T. Abe, K. Itaya, I. Uchida, K. Aoki, K. Tokuda, Bull. Chem. Soc. Jpn. 61 (1988) 3417.
[15] M. Tian, S. Dong, Electroanalysis 7 (1995) 1063.
[16] A. Bond, S. Feldberg, H. Greenhill, P. Mahon, R. Colton, T. Whyte, Anal. Chem. 64 (1992) 1014.
[17] D. Wipf, E. Kristensen, M. Deakin, R.M. Wightman, Anal. Chem. 60 (1988) 306.
[18] M. Mohammad, A. Khan, M. Subhani, N. Murtaza, R. Wahab, S. Malik, J. Electrochem. Soc. India 47 (1998) 214.
[19] R. Nicholson, Anal. Chem. 37 (1965) 1351.
[20] K. Aoki, K. Tokuda, H. Matsuda, J. Electroanal. Chem. 235 (1987) 87.
[21] K. Aoki, Electroanalysis 5 (1993) 627.
[22] K. Oldham, C. Zoski, A. Bond, D. Sweigart, J. Electroanal. Chem. 248 (1988) 467.
[23] A. Bond, K. Oldham, C. Zoski, J. Electroanal. Chem. 245 (1988) 71.
[24] K. Aoki, K. Akimoto, K. Tokuda, H. Matsuda, J. Osteryoung, J. Electroanal. Chem. 171 (1984) 219.
[25] C. Belmont, M.-L. Tercier, J. Buffle, G.C. Fiaccabrino, M. Koudelka-Hep, Anal. Chim. Acta 329 (1996) 203.
[26] W.E. Morf, N.F.d. Rooij, Sensors and Actuators B 44 (1997) 538.
[27] K. Oldham, J. Myland, Fundamentals of Electrochemical Science, Academic Press, New York, 1994.